

Sources of Water in the Taiwan Strait

SEN JAN^{1,4*}, YU-HENG TSENG² and DAVID E. DIETRICH^{2,3}

¹*Institute of Hydrological and Oceanic Sciences, National Central University,
300 Jung-da Rd., Jung-li 32001, Taiwan, R.O.C.*

²*Department of Atmospheric Science, National Taiwan University,
1, Sec. 4, Roosevelt Rd., Taipei 10617, Taiwan, R.O.C.*

³*AcuSea, Inc., 8450-101 Via Sonoma, La Jolla, CA 92037, U.S.A.*

⁴*Institute of Oceanography, National Taiwan University,
1, Sec. 4, Roosevelt Rd., Taipei 10617, Taiwan, R.O.C.*

(Received 2 December 2008; in revised form 13 October 2009; accepted 16 October 2009)

The conveyor of the source water that feeds into the Taiwan Strait (TS), particularly from the south, is investigated using historical CTD (Conductivity-Temperature-Depth) data and a North Pacific Ocean and East Asian seas coupled model. The modeled currents and drifter trajectories suggest that the Kuroshio Branch Water (KBW) rarely flows directly into the TS from the Luzon Strait (LS) in winter; instead the massive westward movement of the Kuroshio conveys high salinity water to the southeastern TS through a loop-like route. In summer, the modeled flow fields suggest that the Kuroshio surface currents hardly intrude into the TS directly from the LS. Observations and model results show that the monsoon-driven northeastward-flowing currents in the northern South China Sea transport relatively low salinity water through the entire TS.

Keywords:

- Water mass,
- conveyor,
- Kuroshio,
- Taiwan Strait,
- Luzon Strait,
- South China Sea.

1. Introduction

The Taiwan Strait (TS) is a 200-km-wide, shallow passage between the island of Taiwan and the China mainland, connecting the South China Sea (SCS) to the East China Sea (ECS). Hydrographic data analyses identify three primary water masses in the TS: the Kuroshio Branch Water (KBW) with high temperature and high salinity, the Mixed China Coastal Water (MCCW), also known as Changjiang Diluted Water, with low temperature and low salinity, and the South China Sea Water (SCSW) with intermediate temperature and salinity (Chu, 1971; Fan and Yu, 1981; Jan *et al.*, 2006a).

Briefly, the SCSW exists primarily in summer (June to September) and is likely carried by the southwest monsoon-driven SCS surface currents from the south to the TS (Fig. 1(a)). The KBW plausibly originates from the Kuroshio's westward intrusion through the Luzon Strait (LS) in late fall to early spring (October to May) and flows northward to the northern TS via the meridional deep channel in the southeastern TS (Fig. 1(b)). There is no doubt that the MCCW originates from the

Changjiang (also known as Yangtze River) diluted water in the Changjiang Estuary (Chen, 2003) and is conveyed by the northeast monsoon-driven, southwest-flowing China Coastal Current to the northern TS during fall to early spring (Fig. 1(b)). The exchange of water mass is modulated by the annual cycle of monsoon forcing, which strengthens the northward current in summer but weakens in other seasons. It is important to note that the TS throughflow transports different water masses, resulting in different heat, salt and material budgets in the ECS, which may thus significantly affect the ECS circulation and hence the biogeochemical budget. Furthermore, numerical tracer experiments conducted by Guo *et al.* (2006) suggest that 50% and 20% of the tracer in the Tsushima (Korea) Strait originates from the TS in summer and winter, respectively. Thus, better understanding of the source water in the TS transcends its local importance.

Compared to the pathway of the MCCW, previous descriptions related to the source and the path of the KBW or SCSW to the TS are mostly speculative (e.g. Nitani, 1972; Fan and Yu, 1981; Shaw, 1989; Jan *et al.*, 2002) due to the lack of integrated investigation between the TS and the northern SCS based on comprehensive field observations. Conceivably, the source water that feeds into the TS from the south must relate to the circulation in the LS and the northern SCS, which is known to be complex

* Corresponding author. E-mail: senjan@ntu.edu.tw

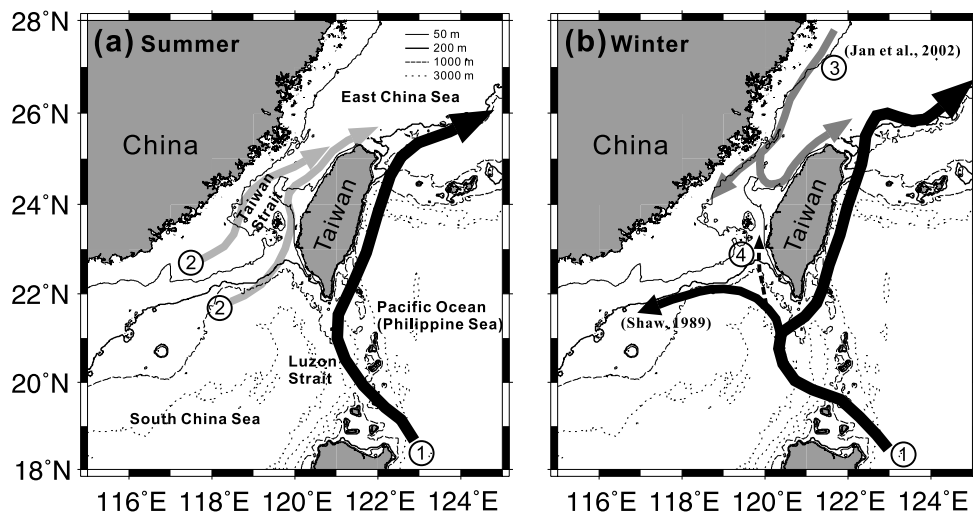


Fig. 1. Bathymetric chart and schematic mean paths of flows entering the Taiwan Strait during (a) summer and (b) winter (1: Kuroshio; 2: Northern SCS surface currents; 3: China Coastal Current; 4: Kuroshio Branch Current).

at seasonal and basin-wide scales. In the LS, the Kuroshio originating east of the Philippines around 15°N may leap or loop across the LS, affecting the circulation and water mass composition in the northern SCS (Shaw, 1989, 1991; Qu *et al.*, 2000; Metzger and Hurlburt, 2001; Centurioni *et al.*, 2004; Ho *et al.*, 2004; Yuan *et al.*, 2006; Du *et al.*, 2008, and others). Based on CTD (Conductivity-Temperature-Depth) data collected in the southwest of Taiwan during May and August, 1986, Shaw (1989) characterized the Kuroshio intrusion water, and proposed that the Kuroshio intrusion may be part of a cyclonic circulation in the northern SCS. Note that the period May through August is defined as part of the summer in this study. Based on the analyses of a large CTD database and oxygen isotope data, Shaw (1991) and Qu (2002) further confirmed that the Kuroshio intrusion water can reach the interior of the SCS in winter. These papers provide early speculation on the conveyor of KBW around the LS.

Using trajectories of the Argos satellite-tracked drifters between 1989 and 2002, Centurioni *et al.* (2004) conclude that the massive westward intrusion of Kuroshio through the LS occurs only in winter (October–January); in other seasons the Kuroshio mostly loops across the LS. Using satellite remote sensing data collected in 1997–2005, Caruso *et al.* (2006) propose that the intrusion in the central region of the LS results in an anticyclonic circulation in the northeastern SCS, while the intrusion in the northern portion of the LS results in a cyclonic circulation. The Kuroshio intrusion water in the northern SCS, i.e. the KBW, identified by Shaw (1991) and Qu (2002) seems to be transported by the massive westward intrusion of Kuroshio in winter examined by Centurioni *et al.* (2004), but with a mean circulation describing an anticy-

clonic rather than a cyclonic loop.

In addition to the seasonal circulation, the strong high-frequency internal waves characterized in the LS to northern SCS (Duda *et al.*, 2004; Jan *et al.*, 2008) are one of the important factors that can increase vertical mixing and then modify the water properties (Jan and Chen, 2009). The energetic eddies revealed by Yuan *et al.* (2006) are also an important factor, transporting and stirring water mass there on a weekly scale. However, evaluating the influence of the factors on the transportation of water mass that enters the TS is beyond the scope of this study, which focuses on the seasonal scale.

The water mass and associated circulation patterns in the TS and LS to the northern SCS have been well studied individually but are rarely discussed and linked together. Hence, this study carefully evaluates the conveyors of the KBW and the SCSW from their source regions, i.e. the LS and the northern SCS, to the TS. A cluster analysis is then applied to the historical CTD data to classify water masses, followed by the model-simulated circulation patterns and drifter trajectories to trace their paths.

2. Water Mass Analysis

2.1 Hydrographic data

The CTD data acquired aboard research vessels Ocean Researcher 1, 2 and 3 (OR-1, 2 and 3 hereafter) covering the area from 114° to 125°E and from 17° to 24°N during 1985 to 2005 were collected for water mass analysis. This domain covers the TS, northern SCS and the LS. The data were seasonally averaged in each $20' \times 20'$ grid and then gridded vertically following the stand-

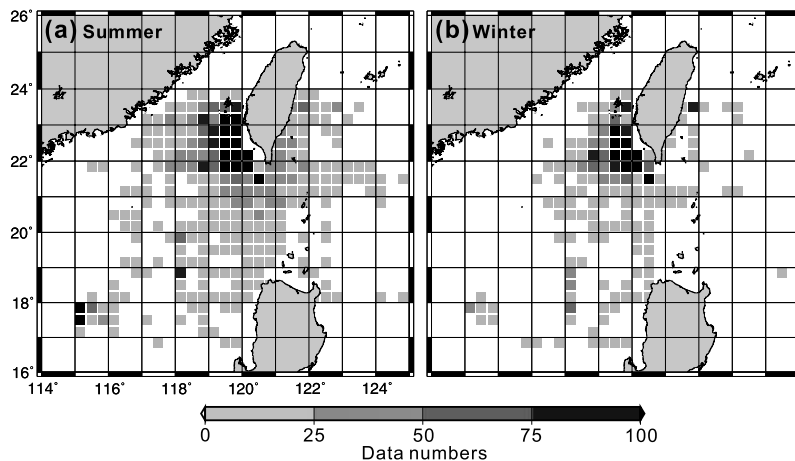


Fig. 2. Numbers of CTD casts in each $20' \times 20'$ grid during (a) summer and (b) winter from 1985 to 2005.

ard depths defined by Levitus and Boyer (1994), viz., 0, 10, 20, 30, 50, 75, 100, 125, 150, 200, 250, 300, 400 and 500 m depths. Only data above 500 m depth were used to analyze the water masses since the depths in the TS are mostly shallower than 100 m. Since the hydrography is significant different between summer (defined as June to August) and winter (December to February), we focus on the results from these two contrasting seasons here. Figure 2 shows the numbers of CTD casts in each grid during summer and winter. Both the density and space coverage of the CTD data are larger in summer than in winter.

The climatological mean currents were compiled by the ship-board acoustic Doppler current profiler (ADCP) data acquired aboard OR-1, 2 and 3 around Taiwan during 1991 to 2007 and can be downloaded from the Ocean Data Bank (<http://140.112.65.17/odbs/Physics/adcp/>) of Taiwan's National Science Council. The current profiler was a 150 kHz ADCP aboard OR-1 and was a 75 kHz ADCP aboard OR-2 and 3. The basic setting indicates that the current velocity was measured every second and a 1–2 min ensemble averaged velocity was stored for applications. The depth bin was normally set to 8–16 m and the measurement depth ranged from 16 to 320 m (Liang *et al.*, 2003). The ship velocity was measured using the ship location positioned by the global positioning system (GPS) when the bottom tracking mode was not available. After debugging, the data were analyzed using the procedure developed by Tang and Ma (1995). Briefly, a 30-min running mean was applied to the data and was set to the mean position of the data. The low-pass-filtered velocity data were then linearly interpolated to the center of a $0.25^\circ \times 0.25^\circ$ grid. In our study area, a grid typically consists of more than 10 data points (see figure 3 in the paper of Liang *et al.*, 2003), which is sufficient to estimate seasonal mean currents. Since the tidal current ve-

locities were not extracted from the raw data, the seasonal mean currents, even though part of the tidal components may be averaged out, are more or less contaminated by tidal currents. Thus the seasonal mean circulation patterns are only described qualitatively here.

2.2 Cluster analysis

The water mass classification was performed with a cluster analysis and associated T-S diagrams. The cluster analysis is not merely a typical statistical procedure; rather, it is a collection of different algorithms that put objects into clusters according to the well-defined similarity rules (Wilks, 1995). The advantage of the cluster analysis is that it enables objects of similar kinds to be gathered into respective categories from massive data such as the CTD data in this study. Similar to the cluster analysis used by Hur *et al.* (1999), our method is based on a criterion coefficient (F), defined as

$$F = (\Delta T/\sigma_T)^2 + (\Delta S/\sigma_S)^2 + (\Delta D/\sigma_D)^2 + L/L_c, \quad (1)$$

where T , S and D stand for the mean temperature, salinity and depth of a cluster, respectively; σ_T , σ_S and σ_D denote standard deviations for temperature, salinity and depth of the data set; L and L_c represent geographical distance and a characteristic distance scale, respectively. As can be seen, the smaller the value of F , the closer the two clusters are. The value of characteristic distance L_c (40 km in this study) depends primarily on the horizontal resolution of the CTD data (~ 36 km). Thus when $L = 40$ km, it contributes to one standard deviation of the factor F . A sample mean is applied to calculate the temperature, salinity and depth for each cluster. The geographical distance is defined as the shortest distance between two clusters in order to enable a throughflow feature to be discerned by cluster analysis (Wilks, 1995). The value of F

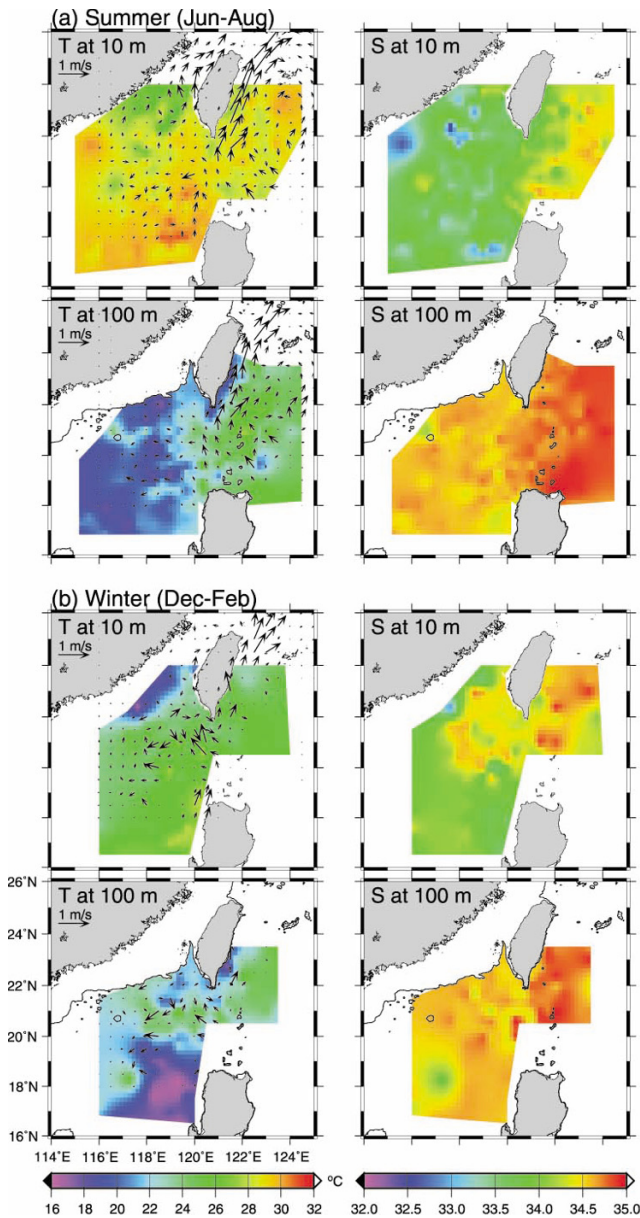


Fig. 3. Seasonal mean temperature and salinity distributions at 10 and 100 m depths for (a) summer and (b) winter.

is set to 1.5 here, which means when F between two data (or clusters) is less than 1.5, they are grouped together.

Based on the definition, the procedure of a cluster analysis begins from the comparison of an arbitrary picked CTD datum (base datum) with the other data. Once the F calculated from the base datum and some other datum is smaller than 1.5, the two data are grouped into a new cluster. The aforementioned grouping process is applied to the new cluster. The first run of the procedure is then completed when each datum is compared with the first cluster; the statistics of the cluster such as the mean tempera-

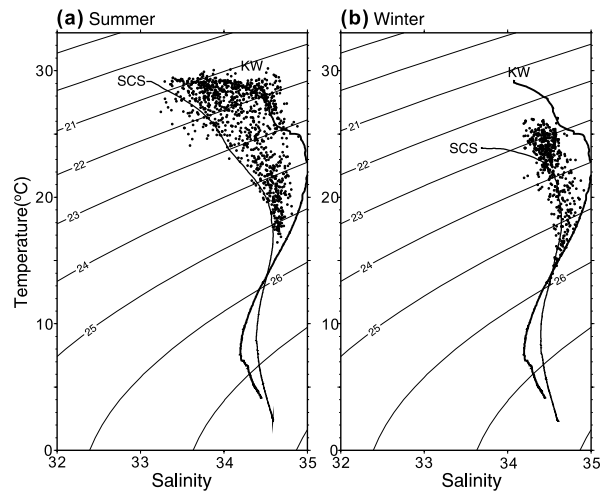


Fig. 4. T-S diagram of the processed CTD data in (a) summer and (b) winter.

Table 1. Properties of water masses classified by the cluster analysis. T , S and D stand for seasonal mean temperature, salinity and depth of each water mass.

Season	Water mass	T (°C)	S	D (m)
Summer	SCSW	27.66	33.92	21.3
	KBW	24.63	34.49	62.8
Winter	KBW	20.54	34.59	115.8

ture, salinity and depth and the depth range of the grouped data are then calculated. The same procedure is applied to the remaining data until the data cannot be grouped to each other.

2.3 Seasonal water mass distribution

Note that winds over the northern SCS, TS and LS are dominated by the East Asian monsoon, which is southwesterly with averaged speed of about 5 m/s in summer and northeasterly with averaged speed of up to 10 m/s in winter. The circulation and hydrography in these regions are normally subject to the seasonal change of the prevailing winds. The seasonal mean temperature and salinity distributions at 10 and 100 m depths for summer and winter are shown in Fig. 3, superimposed by the seasonal mean current velocity analyzed from the historical shipboard ADCP data. These depths are chosen to represent surface and subsurface layers, respectively. In summer (Fig. 3(a)), the surface (10 m depth) temperature is lower ($<29^{\circ}\text{C}$) from the southern TS to northern SCS and east of LS and Taiwan. The higher temperature presents west of LS in the area between $118\text{--}120^{\circ}\text{E}$ and east of 123°E .

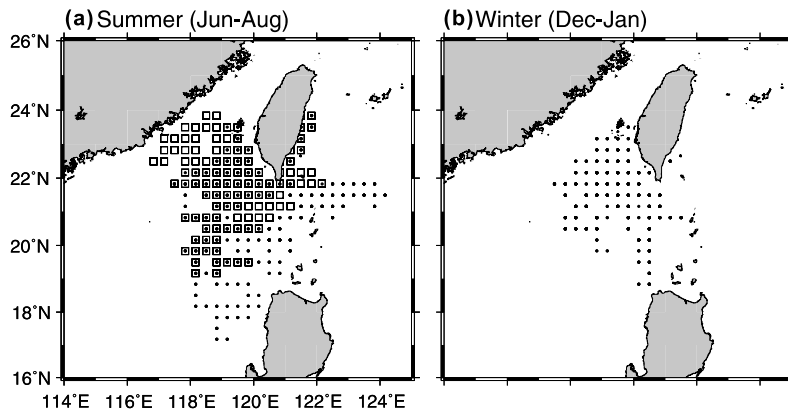


Fig. 5. Horizontal distribution of the major water masses classified by cluster analysis during (a) summer and (b) winter. Open square and solid circle represent SCSW and KBW, respectively.

The surface salinity is higher (>34.5) roughly east of 121°E , but relatively lower (<34) along the east coast of Taiwan and in the northern SCS. The Kuroshio water and its associated circulation pattern in the northern SCS are not easily identified from the surface hydrographic pattern in summer. In comparison, it is easily seen from the hydrographic pattern of the subsurface layer (100 m depth in Fig. 3(a)) that the warmer ($>24^{\circ}\text{C}$) and more saline (>34.5) Kuroshio water occupies the LS east of 120°E . In winter (Fig. 3(b)), the surface temperature is around 25°C except for the southwestern TS where the temperature is lower than 20°C . The surface salinity distribution indicates that the saline water extends far further west to $\sim 117^{\circ}\text{E}$ and the southeastern TS compared to conditions in summer. The warmer water in the subsurface layer also likely extends to the west, but the distribution of the subsurface salinity remains similar pattern to that in summer.

Figure 4 shows the T-S diagram for the gridded seasonal mean CTD data in summer and winter. The T-S curves of the typical SCSW and Kuroshio water (KW) are plotted on Fig. 4 for reference; the T-S data for the two typical water masses were from the CTD casts in the central part of the northern SCS (115.67°E , 18.25°N) and the Kuroshio region (123.00°E , 19.00°N), respectively. The temperature and salinity in summer spread in a wider range between the T-S curves of the SCSW and the KW than those in winter, suggesting that the characteristics of water masses in the northern SCS are complicated in summer. However, both Figs. 3 and 4 provide no further objective information on the property of the water mass in the study area.

The cluster analysis is further used to classify the water mass. Preliminary results indicated that each season could include up to five groups, but only groups of significant data quantity and space coverage are shown

and discussed below. The results of the cluster analysis suggest that two distinct groups of water mass, i.e. the SCSW and subsurface KBW (the SB-KBW in Jan *et al.*, 2006a), were classified in summer; only one primary group of water mass was classified in winter. Table 1 summarizes the properties of the three water masses. The warmer (27.66 vs. 24.63°C) but less saline (33.92 vs. 34.49) SCSW exists in shallower depths than KBW (21.3 vs. 62.8 m) in summer, while in winter the saline KBW (34.59) dominates the water mass in the northern SCS at depth 115.8 m. These properties are consistent with the statement that the source water in the TS comes from the SCSW in summer but potentially comes from the KBW in winter. Figure 5 shows the horizontal extent of each water mass in summer and winter, respectively. In summer, the SCSW (open square in Fig. 5) with mean temperature 27.66°C and salinity 33.92 occupies the surface layer with a mean depth 21.3 m in the junction area between the TS and northern SCS. Notably, some of the surface SCSW extends to the east coast of Taiwan (Fig. 5(a)). The other one is the KBW (solid circle in Fig. 5) with relatively lower mean temperature 24.63°C and higher salinity, 34.49 , distributed primarily in the LS and below the SCSW in the northern SCS. The average depth of the KBW is 62.8 m, which is deeper than that of the SCSW in summer. In winter, the major water mass, the KBW, with the lowest mean temperature 20.54°C and the highest salinity 34.59 resides in the LS and the northern SCS with mean depth 115.8 m. Based on the distribution of high-salinity water in Figs. 3(b) and 5(b), it can easily be inferred that the route of the KBW in winter moves directly from the LS towards the southeastern TS, as shown schematically in Fig. 1(b). Shaw (1989) also suggested that the KBW was brought by part of a cyclonic gyre in the northern SCS in winter. However, previous speculation on the conveyor of the KBW in winter (see

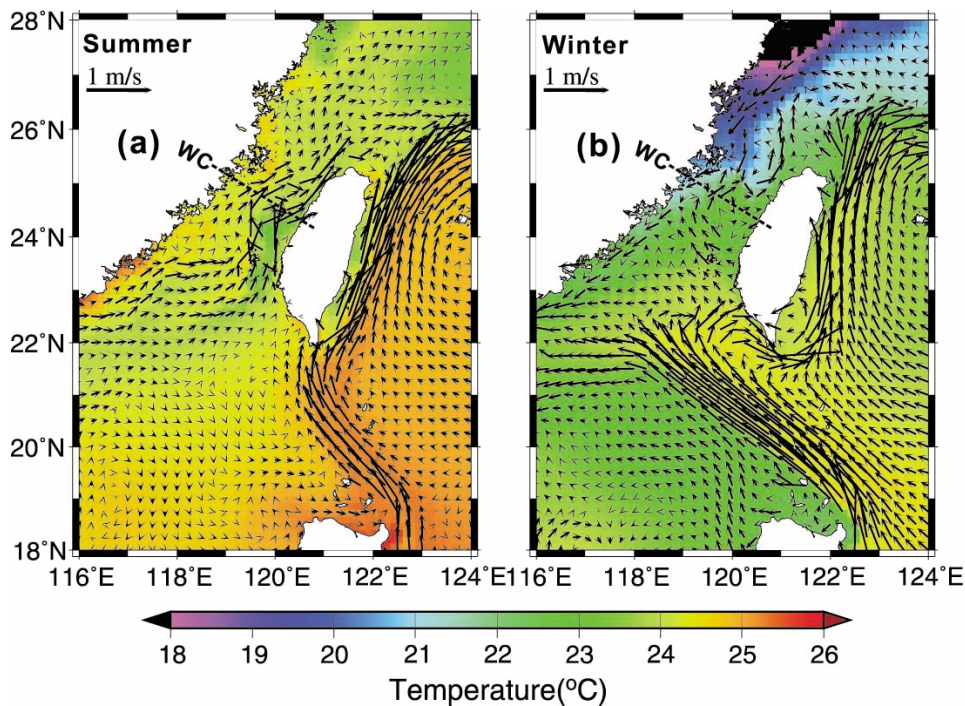


Fig. 6. Seasonal mean surface flow (layers 1 and 2 averaged) and corresponding surface temperature for (a) July–August and (b) January–February of model year 38.

Fig. 1(b)) is not supported by the results derived from our numerical drifter experiment, which is discussed below.

3. Numerical Experiment and Discussion

3.1 Model description

The duo-grid Pacific Ocean model (DUPOM) used in this study is revised from the fourth-order accurate, collocated Arakawa-A grid DieCAST (Dietrich/Center for Air Sea Technology) model (Dietrich, 1997; Dietrich *et al.*, 2004a; Tseng *et al.*, 2005), which was first described by Jan *et al.* (2006b). The control volume equations include fluxes of the conservation properties (momentum, heat and salt) across control volume faces. The model domain covers the entire North Pacific Ocean ranging from 30°S to 60°N and from 100°E to 80°W. To reduce computational time, a duo-grid approach is used according to a multiple-grid framework described by Dietrich *et al.* (2004a) and Dietrich *et al.* (2008). A $1^\circ/8$ resolution is used in the domain west of 150°E where it is necessary to resolve the detailed regional circulations; a $1^\circ/4$ resolution is used in the domain east of 150°E. The grids are fully two-way-coupled, each coarser time step (different time steps are used for both grids) with a single coarse grid overlapping (i.e. 2×2 in fine grid cells). The meander and eddy exchanges are seamless at the interface without inter-grid sponge layers or special treat-

ment. Further details of the multiple-grid approach can be found in Dietrich *et al.* (2008).

Model bathymetry is established using unfiltered 2-min (~ 3.6 km) ETOPO2 depth data (<http://www.ngdc.noaa.gov/mgg/global/relief/ETOPO2/ETOPO2v2-2006/ETOPO2v2c/>) supplemented with 1-min (~ 1.8 km) depth archive in the Asian seas from Taiwan's Ocean Data Bank. The vertical resolution is linear-exponentially stretched by 26 levels. The layer thickness varies from 13.28 m in the top layer to 891.02 in the bottom layer. The vertical mid-points of the layers are at depths 6.46, 20.51, 36.34, 54.35, 75.02, 98.94, 126.82, 159.55, 198.20, 244.07, 298.77, 364.26, 442.91, 537.65, 652.04, 790.43, 958.13, 1161.62, 1408.85, 1709.48, 2075.34, 2520.88, 3063.73, 3725.44, and 4532.33 m. These vertical levels are used in both the coarser and finer grids. Within each horizontal grid in each domain, zonal resolution is uniform and meridional resolution is specified such that each control volume is approximately square (Mercator grid); thus, the model control volumes decrease with increasing latitude as do the typical ocean eddy sizes.

Since this study is to evaluate the pathway of source water from the south in seasonal scale, the Hellerman and Rosenstein wind stresses (Hellerman and Rosenstein, 1983) and the Levitus 94 climatology (Levitus and Boyer, 1994) were easily adopted to spin up the model. The surface wind forcing is obtained from the interpolated

monthly Hellerman and Rosentstein's wind stresses. The Levitus 94 climatology is used to initialize the model and determine its surface sources of heat and fresh water (evaporation minus precipitation) using the non-damping approach described in Dietrich *et al.* (2004b). The northern boundary is closed. The southern boundary condition (30°S) is slowly nudged toward climatology in a sponge layer. The bottom is insulated, with no-slip conditions parameterized by a nonlinear bottom drag. Sub-grid scale vertical mixing is parameterized by eddy diffusivity and viscosity using a modified Richardson-number-dependent formula (Staneva *et al.*, 2001; Tseng *et al.*, 2005) based on Pacanowski and Philander (1981). Background lateral viscosity (or diffusivity) is 100 and 20 m²/s in both domains. Since this is a fourth-order accuracy, low-dissipation model, it took ~10 model years to reach a quasi-cyclic (annually) equilibrium state. Simulated results after model year 30 are stored for application.

The simulated flow patterns in the Asian seas have been validated by Du *et al.* (2008), and these agree reasonably with the observations. For example, the model-produced annual throughflow transport at a zonal section along 24.5°N east of Taiwan, 22.1 Sv (1 Sv = 10⁶ m³/s) (integrated from 121.8 to 125°E and from 1000 m depth to the surface) is comparable with the observed mean transport, 21 ± 2.5 Sv, across a similar section, the PCM-1 section, during the World Ocean Circulation Experiment (WOCE) from September 1994 to May 1996 (Johns *et al.*, 2001). The temporal variation of the simulated transport is also consistent with that observed at the section. The three-layered throughflow transport structure observed by Tien *et al.* (2006) in the LS is successfully reproduced in our model.

Particular model-data comparisons focus on the circulation in the TS. Figure 6 shows the seasonal mean surface (levels 1 and 2 averaged) current velocity and temperature for summer and winter of year 38, which are regarded as seasonal circulation patterns. The qualitative similarity between our model-produced flow pattern and the observed seasonal mean current distribution plotted in Fig. 3 is clear, especially in the regions around Taiwan and its vicinity. The main stream of the Kuroshio curves at ~0.5 m/s across the LS in summer, but with a more westward loop it intrudes to the northern SCS more in winter than in summer. Besides the looped warm Kuroshio, the mean summer surface currents in Fig. 6(a) show that there is a relatively cold northeastward flow on the continental shelf south of China. Part of the flow branches into the southwestern TS at ~117°E and part of it reaches the southeastern TS. The mean winter currents in Fig. 6(b) indicate that the Kuroshio intrusion reaches ~118°E in the northern SCS and turns anticyclonically back toward the southern tip of Taiwan. At 118°E, part of

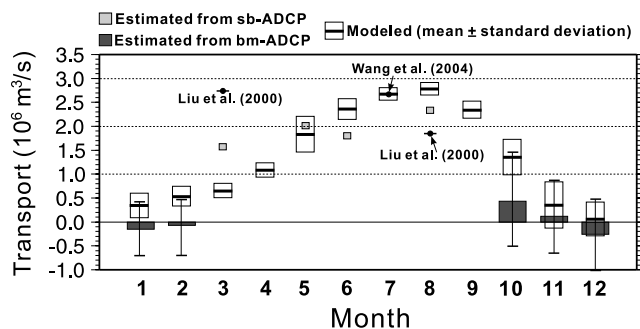


Fig. 7. Simulated and observed monthly mean throughflow (section WC in Fig. 6) transport in the Taiwan Strait.

the intruded Kuroshio separates from its main loop flowing toward the west. Consistent with the findings of Wang and Chern (1988), the westward intrusion of the Kuroshio, particularly in winter, forms an anticyclone in the northern SCS.

Figure 7 shows the observed and modeled monthly mean throughflow transports in the TS. The observed values were estimated from shipboard ADCP data obtained during a few one-week cruise observations and long-term moored ADCP measurements in the middle section of TS. The detailed observation and data processing methods are described in Jan *et al.* (2006a). Considering uncertainties in measurement and model, comparison with Fig. 7 suggests that the modeled transports agree quantitatively with the observed ones, as well as the values summarized in Isobe (2008). That is, associated with the change of East Asia monsoon, the northeastward transport increases in spring and summer, peaks in early fall (August) and weakens thereafter. During the strongest northeast monsoon period (December and January), the monthly throughflow transport sometimes reverses towards the south. The monthly mean transports derived from the modeled currents are positive in December, January and February, which differs from the observations. The truncation error of the coastline due to coarse grid resolution and smoothness of the climatologic wind stress are possible sources for the discrepancy. Nonetheless, the simulated transports are weak in winter and within a standard deviation of the observed monthly mean transports.

3.2 Conveyor of water mass

In order to trace the source water entering the TS from the south, a series of lagrangian drifter experiments was performed using the validated flow fields described in Subsection 3.1. The drifters were released at 20.51, 54.35 and 98.94 m depth over the continental shelf in the northern SCS along 115.38, 116.38 and 117.28°E and across the LS along 120.5, 120 and 121.5°E. Each drifter was deployed at 0 h on the first day of January, March,

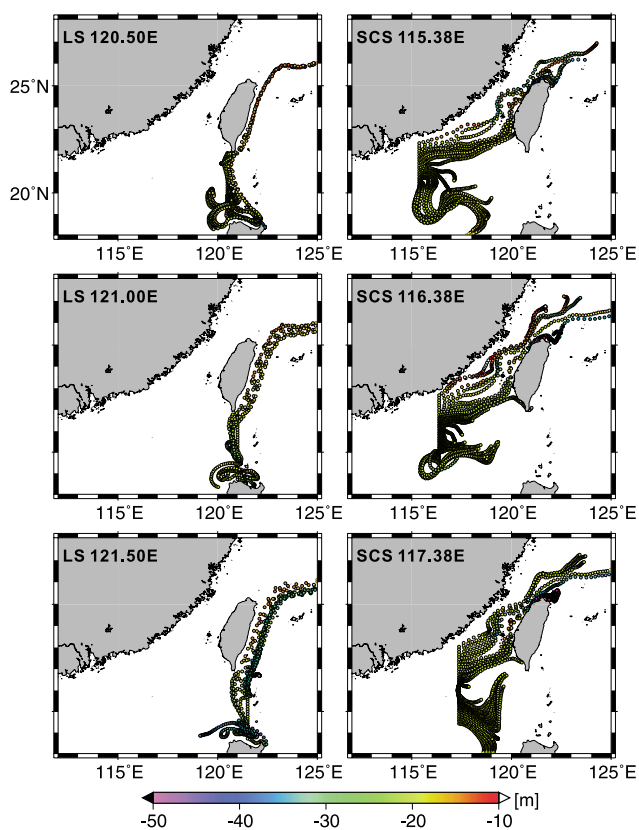


Fig. 8. Simulated drifter trajectories for summer (July–August). Depth of the drifter is indicated by colors.

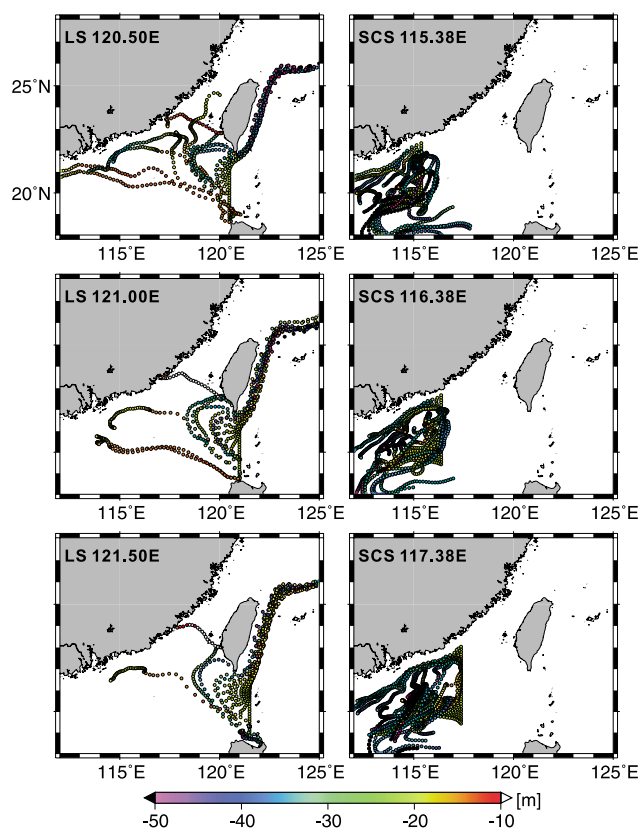


Fig. 9. As Fig. 8 but for winter (January–February).

May, July, September and November. The daily position and corresponding depth of each drifter within two months after deployment were stored for analysis. Since the simulated horizontal trajectories present low differences between drifters deployed at the three depths, we only demonstrate results from 20.51 m depth. The simulated trajectories during July to August and January to February, corresponding to summer and winter, respectively, are discussed below.

Figure 8 shows the drifter trajectories during summer. The change of depth during the drifting of each drifter is represented by colors. Overall, the simulated trajectories starting from the LS are qualitatively consistent with those of the Argos satellite-tracked drifters compiled in Centurioni *et al.* (2004; their figures 2 and 4). Figure 8 indicates that, in July to August, the majority of drifters released along the three meridional sections in the LS drift northward with the main stream of Kuroshio in the east of Taiwan. No drifters reach the northern SCS. This indicates that the high salinity Kuroshio water can hardly be transported into the TS during summer. On the other hand, about half of the drifters deployed along the three sections in the northern SCS enter the TS through both the

shallow bank and the deep meridional channel in the southern TS. The drifters that move into TS merge in the northeastern TS then drift to the East China Sea. The model-simulated drifter trajectories lend support to the previous suggestion regarding the replacement of the KBW by the SCSSW in the TS during summer (Fan and Yu, 1981).

Figure 9 shows the drifter trajectories during winter. Compared with Fig. 8, the drifter trajectories in Fig. 9 are more complex and are seemingly reversed in direction. The distinct feature is that drifters deployed along the three sections in the northern SCS essentially drift southwestward. It suggests that the SCS shelf water is hardly transported to the TS during the two months. Trajectories of drifters released from the three sections in the LS vary, but can roughly be grouped into three categories. The drifters deployed in the southern portion of the LS move westward accompanying the cyclonic circulation in the SCS; some of them deployed along 120.5°E can reach as far as west of 112°E. The drifters deployed in the middle reaches of the LS curve anticyclonically in the northeastern SCS and branch when approaching southwest coast of Taiwan. Most of them pass around the south-

ern tip of Taiwan then drift along the east coast of Taiwan. The other drifters turn towards the west across the southern TS. This is likely the primary pathway transporting the KBW to the southern TS in winter. The drifters deployed in the northern portion of the LS simply drift northward with the Kuroshio. The simulated trajectories in winter provide useful information for evaluating the pathway of the westward intrusion of Kuroshio.

Wang and Chern (1988) proposed that the Kuroshio westward-intrusion via the LS in winter may accumulate and establish an anticyclonic warm core circulation in the northern SCS. When the northeast monsoon weakens in early spring, the KBW could intrude northward through the TS. However, Nitani (1972) and Shaw (1989) speculated that the warm, saline water originating from the Kuroshio enters the TS directly from the northern LS in winter, as shown schematically in Fig. 1(b). Shaw (1989), contrary to Wang and Chern's (1988) viewpoint, proposed that the Kuroshio intrusion may be part of a cyclonic gyre in the northern SCS. The simulated wintertime flow field and associated surface temperature in Fig. 6(b) tend to agree with Wang and Chern's (1988) suggestion. Indeed, an anticyclonic circulation in the northern SCS in winter was also characterized from observed trajectories of satellite-tracked drifters (Centurioni *et al.*, 2004) and model simulations (e.g. Metzger and Hurlburt, 1996, 2001).

3.3 Discussion

It is worth mentioning that the existence of a permanent throughflow in the TS is a matter of debate. Yang (2007) stated that a persistent northeastward current exists in the TS throughout the year, despite the strong southwestward wind stress in winter. Using a simplified numerical model, Yang attributed the driving mechanism to the Kuroshio-built northward pressure gradient between both ends of the TS. By contrast, Chen and Sheu (2006) analyzed CTD, oxygen isotope ($\delta^{18}\text{O}$), satellite sea surface temperature and Argos satellite-tracked drifter data collected in the TS and concluded that, in winter, the warmer water from northern SCS reach only the southern part of the TS without flowing further north through the northern TS. The hydrographic observations and satellite sea surface temperature indicate that a zonal oceanic front is frequently observed in the central TS in winter (Li *et al.*, 2006), which agrees with Chen and Sheu's (2006) conclusion. Our numerical result described herein further clarifies the controversy, suggesting that there is hardly a persistent northeastward warm current in the TS against the strong northeast monsoon in winter (Figs. 6(b) and 9).

Although it may serve some useful purpose, there are limitations to the conveyor belt theory. In the present application, the major seasonal wind forcing changes that control the Taiwan Strait, even on a seasonal timescale in

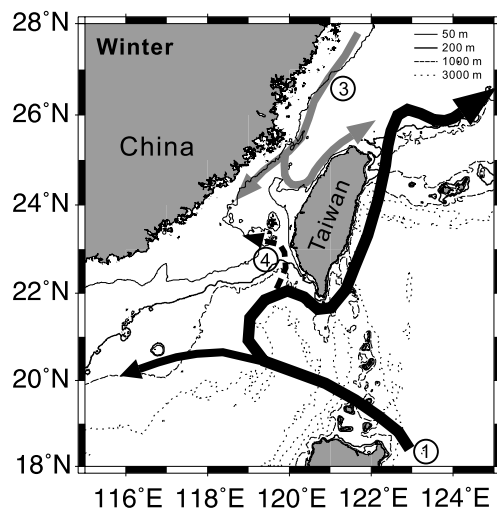


Fig. 10. As Fig. 1(b) but with revision derived from this study.

the upper ocean near Taiwan, do not result in all of the water mass formed during the previous season being flushed out of the regions affecting the Taiwan Strait, thus adding complexity to seasonal water mass source analysis.

In addition to the concern described above, the behavior of the Kuroshio in the LS varies significantly in seasonal and intra-seasonal scales (Centurioni *et al.*, 2004; Yuan *et al.*, 2006) and in turn significantly modifies the property of the water mass in the northern SCS. The dynamics of the Kuroshio variability in this region are subject to debate (e.g. Shaw 1989, 1991; Metzger and Hurlburt, 1996, 2001; Sheremet, 2001) and this is still one of the contemporary issues related to the complicated oceanic processes in the LS. Nevertheless, this study serves as a modest start evaluating the conveyor of the source water feeding into the TS on the basis of reasonable model-simulated circulations in the East Asian seas.

4. Summary

The water mass in the TS consists of the MCCW, SCSW and KBW in different seasons. Doubtless, the cold, brackish MCCW originates in the Changjiang river mouth and the East China Sea shelf and is driven southward by the northeast monsoon into the northern TS in winter. The conveyors of the SCSW and KBW from the northern SCS or the LS to the TS have yet to be clarified. The integrated information from the water mass distribution (Fig. 5), observed and simulated seasonal mean flow fields (Figs. 3 and 6), and simulated drifter trajectories (Figs. 8 and 9) suggests that the KBW hardly intrudes northward to the TS in summer. In winter, our simulation indicates that part of the looped Kuroshio could reach southeastern TS rather than directly intrude into the TS from the

LS. Meanwhile, the less saline northern SCS shelf water cannot reach the TS. Based on the evaluation, Fig. 10 shows the revised conveyor of the KBW (cf. Fig. 1(b)) intrusion to the southern TS in winter.

In summary, water mass classification using a cluster analysis and a two-way-coupled duo-grid North Pacific Ocean model have been adopted to examine and clarify the conveyor of the source water that supplies the TS from the south. The simulated flow field suggests that the near Kuroshio surface current rarely flows directly into the TS from the LS in winter; instead, the massive westward intrusion of the Kuroshio forms a loop-like path in the northern SCS and provides high salinity water (KBW) to the southeastern TS. The simulated drifter trajectories suggest that, during the strong northeast monsoon season, the KBW cannot flow further northeastward through the TS. In summer, the simulated drifter trajectories indicate that the Kuroshio surface current in the LS hardly reaches the southeastern TS. Instead, the northeastward-flowing currents on the continental shelf south of China transport the less saline SCSSW through the TS. Results derived from the cluster analysis and the model-simulated flow field and drifter trajectories depict the pathway of the source water that enters the TS.

Acknowledgements

This study is funded by Taiwan's National Science Council (NSC) under grant NSC95-2611-M-008-004-MY3. Two anonymous reviewers and the editor provided constructive criticisms which helped improve the paper. Y.-H. Tseng acknowledges the supported by the NSC under grant NSC96-2628-M-002-010. D. Dietrich was sponsored by the NSC during October 2007 to February 2008. The Ocean Data bank of the NSC provided bathymetry, historical CTD and climatological current data analyzed from historical ship-board ADCP data. J.-K. Hu, C.-C. Chiou, S.-H. Chen and S.-H. Chien assisted part of this study. The Taiwan's National Center for High-performance Computing offered an allocation of computer time and facilities.

References

- Caruso, M. J., G. G. Gawarkiewicz and R. C. Beardsley (2006): Interannual variability of the Kuroshio intrusion in the South China Sea. *J. Oceanogr.*, **62**(4), 559–575.
- Centurioni, L. R., P. P. Niiler and D. K. Lee (2004): Observations of inflow of Philippine Sea surface water into the South China Sea through the Luzon Strait. *J. Phys. Oceanogr.*, **34**, 113–121.
- Chen, C.-T. A. (2003): Rare northward flow in the Taiwan Strait in winter: a note. *Cont. Shelf Res.*, **23**, 387–391, doi:10.1016/S0278-4343(02)00209-1.
- Chen, C.-T. A. and D. D. Sheu (2006): Does the Taiwan Warm Current originate in the Taiwan Strait in winter-time? *J. Geophys. Res.*, **111**, C04005, doi:10.1029/2005JC003281.
- Chu, T.-Y. (1971): Environmental study of the surrounding waters of Taiwan. *Acta Oceanogr. Taiwanica*, **1**, 15–32.
- Dietrich, D. E. (1997): Application of a modified Arakawa 'a' grid ocean model having reduced numerical dispersion to the gulf of Mexico Circulation. *Dyn. Atmos. Oceans*, **27**, 201–217.
- Dietrich, D. E., A. Mehra, R. L. Haney, M. J. Bowman and Y.-H. Tseng (2004a): Dissipation effects in North Atlantic Ocean modeling. *Geophys. Res. Lett.*, **31**, L05302, doi:10.1029/2003GL019015.
- Dietrich, D. E., R. L. Haney, V. Fernandez, S. A. Josey and J. Tintore (2004b): Air-sea fluxes based on observed annual cycle surface climatology and ocean model internal dynamics: A precise, non-damping zero-phase-lag approach applied to the Mediterranean Sea. *J. Mar. Sys.*, **52**, 145–165.
- Dietrich, D. E., Y. H. Tseng, R. Medina, M. Liste, M. Olabarriet, S. A. Piacsek, M. J. Bowman and A. Mehra (2008): Accurate Mediterranean overflow water (MOW) simulation using a coupled multiple-grid Mediterranean Sea/North Atlantic Ocean model on a PC. *J. Geophys. Res.*, **113**, C07027, doi:10.1029/2006JC003914.
- Du, T., Y.-H. Tseng and X. H. Yan (2008): The generation of internal waves under different flow conditions in Luzon Strait. *J. Geophys. Res.* **113**, C08015, doi:10.1029/2007JC004294.
- Duda, T. F., J. F. Lynch, J. D. Irish, R. C. Beardsley, S. R. Ramp, C.-S. Chiu, T.-Y. Tang and Y.-J. Yang (2004): Internal tide and nonlinear internal wave behavior at the continental slope in the northern South China Sea. *IEEE J. Oceanic Eng.*, **29**(4), 1105–1130.
- Fan, K.-L. and C.-Y. Yu (1981): A study of water masses in the seas of southernmost Taiwan. *Acta Oceanogr. Taiwanica*, **12**, 94–111.
- Guo, X., Y. Miyazawa and T. Yamagata (2006): The Kuroshio onshore intrusion along the shelf break of the East China Sea: The origin of the Tsushima Warm Current. *J. Phys. Oceanogr.*, **36**, 2205–2231.
- Hellerman, S. and M. Rosenstein (1983): Normal monthly wind stress over the world ocean with error estimates. *J. Phys. Oceanogr.*, **13**, 1093–1104.
- Ho, C.-R., Q. Zheng, N.-J. Kuo, C.-H. Tsai and N. E. Huang (2004): Observation of the Kuroshio intrusion region in the South China Sea from AVHRR data. *Int. J. Remote Sen.*, **25**(21), 4583–4591.
- Hur, H. B., G. A. Jacobs and W. J. Teague (1999): Monthly variations of water masses in the Yellow and East China Seas. *J. Oceanogr.*, **55**, 171–184.
- Isobe, A. (2008): Recent advances in ocean-circulation research on the Yellow Sea and East China Sea shelves. *J. Oceanogr.*, **64**, 569–584.
- Jan, S. and C.-T. A. Chen (2009): Potential biogeochemical effects from vigorous internal tides generated in the Luzon Strait: A case study at the southernmost coast of Taiwan. *J. Geophys. Res.-Oceans*, **114**, C04021, doi:10.1029/2008JC004887.
- Jan, S., J. Wang, C.-S. Chern and S.-Y. Chao (2002): Seasonal variation of the circulation in the Taiwan Strait. *J. Mar. Sys.*, **35**, 249–268, doi:10.1016/S0924-7963(02)00130-6.

- Jan, S., D. D. Sheu and H.-M. Kuo (2006a): Water mass and throughflow transport variability in the Taiwan Strait. *J. Geophys. Res.*, **111**, C12012, doi:10.1029/2006JC003656.
- Jan, S., D. E. Dietrich, Y.-H. Tseng and Y. Yang (2006b): Development of a low-dissipation, high-computational-efficiency Duo Grid Pacific Ocean Model (DUPOM). *Eos Trans. AGU*, **87**(36), Ocean Sci. Meet. Suppl., Abstract OS46F-15.
- Jan, S., R.-C. Lien and C.-H. Ting (2008): Numerical study of baroclinic tides in Luzon Strait. *J. Oceanogr.*, **64**(5), 789–802.
- Johns, W. E., T. N. Lee, D. Zhang, R. Zantopp, C.-T. Liu and Y. Yang (2001): The Kuroshio east of Taiwan: Moored transport observations from the WOCE PCM-1 array. *J. Phys. Oceanogr.*, **31**, 1031–1053.
- Levitus, S. and T. P. Boyer (1994): *World Ocean Atlas 1994. Vol. 4: Temperatures*. NOAA Atlas NESDIS, U.S. Department of Commerce, Washington, D.C.
- Li, C., J. Hu, S. Jan, Z. Wei, G. Fang and Q. Zheng (2006): Winter–spring fronts in Taiwan Strait. *J. Geophys. Res.*, **111**, C11S13, doi:10.1029/2005JC003203.
- Liang, W.-D., T. Y. Tang, Y. J. Yang, M. T. Ko and W.-S. Chuang (2003): Upper-ocean currents around Taiwan. *Deep-Sea Res. II*, **50**, 1085–1105.
- Metzger, E. J. and H. E. Hurlburt (1996): Coupled dynamics of South China Sea, the Sulu Sea, and the Pacific Ocean. *J. Geophys. Res.*, **101**, 12331–12352.
- Metzger, E. J. and H. E. Hurlburt (2001): The nondeterministic nature of Kuroshio penetration and eddy shedding in the South China Sea. *J. Phys. Oceanogr.*, **31**, 1712–1732.
- Nitani, H. (1972): Beginning of the Kuroshio. p. 353–369. In *Kuroshio: Its Physical Aspects*, ed. by H. Stommel and K. Yoshida, Univ. of Tokyo Press, Tokyo.
- Pacanowski, R. C. and S. G. H. Philander (1981): Parameterization of vertical mixing in numerical models of tropical oceans. *J. Phys. Oceanogr.*, **11**, 1443–1551.
- Qu, T. (2002): Evidence of water exchange between the South China Sea and the Pacific through the Luzon Strait. *Acta Oceanol. Sinica*, **21**, 175–185.
- Qu, T., H. Mitsudera and T. Yamagata (2000): Intrusion of the North Pacific waters into the South China Sea. *J. Geophys. Res.*, **105**, 6415–6424.
- Shaw, P.-T. (1989): The intrusion of water masses into the sea southwest of Taiwan. *J. Geophys. Res.*, **94**, C12, 18213–18226.
- Shaw, P.-T. (1991): Seasonal variation of the intrusion of the Philippine sea water into the South China Sea. *J. Geophys. Res.*, **96**, 821–827.
- Sheremet, V. (2001): Hysteresis of a western boundary current leaping across a gap. *J. Phys. Oceanogr.*, **31**, 1274–1259.
- Staneva, J. V., D. E. Dietrich, E. V. Stanev and M. J. Bowman (2001): Rim current and coastal eddy mechanisms in an eddy-resolving Black Sea general circulation model. *J. Mar. Sys.*, **31**, 137–157.
- Tang, T. Y. and J. C. Ma (1995): A note on the accuracy of shipboard ADCP on Ocean Research I. *Acta Oceanogr. Taiwanica*, **34**, 71–81.
- Tien, J., Q. Yang, X. Liang, L. Xie, D. Hu, F. Wang and T. Qu (2006): Observation of Luzon Strait transport. *Geophys. Res. Lett.*, **33**, L19607, doi:10.1029/2006GL026272.
- Tseng, Y.-H., D. E. Dietrich and J. H. Ferziger (2005): Regional circulation of the Monterey Bay region-hydrostatic versus non-hydrostatic modeling. *J. Geophys. Res.*, **110**, C09015, doi:10.1029/2003JC002153.
- Wang, J. and C.-S. Chern (1988): On the Kuroshio branch in the Taiwan Strait during wintertime. *Prog. Oceanogr.*, **21**, 469–491.
- Wilks, D. S. (1995): *Statistical Methods in the Atmospheric Sciences: An Introduction*. Academic Press, New York, 428 pp.
- Yang, J. (2007): An oceanic current against the wind: How does Taiwan Island steer warm water into the East China Sea? *J. Phys. Oceanogr.*, **37**, 2563–2569, doi:10.1175/JPO3134.1.
- Yuan, D., W. Han and D. Hu (2006): Surface Kuroshio path in the Luzon Strait area derived from satellite remote sensing data. *J. Geophys. Res.*, **111**, C11007, doi:10.1029/2005JC003412.